ADVANCED MATERIALS

Supporting Information

for *Adv. Mater.*, DOI: 10.1002/adma.201302660

Ultrahigh Thermoelectric Performance by Electron and Phonon Critical Scattering in $Cu_2Se_{1-x}I_x$

Huili Liu, Xun Yuan, Ping Lu, Xun Shi, Fangfang Xu, Ying He, Yunshan Tang, Shengqiang Bai, Wenqing Zhang,* Lidong Chen,* Yue Lin, Lei Shi, He Lin, Xingyu Gao, Xingmin Zhang, Hang Chi, and Ctirad Uher*

Submitted to ADVANCED MATERIALS

Supporting information for

Ultrahigh Thermoelectric Performance by Electron and Phonon Critical Scattering in $Cu_2Se_{1-x}I_x$

By *Huili Liu*[1,2†], *Xun Yuan*[1,2†], *Ping Lu*[1,2], *Xun Shi*[1,3*], *Fangfang Xu*[1], *Ying He*[1,2], *Yunshan Tang*[3], *Shengqiang Bai*[3], *Wenqing Zhang*[1*], *Lidong Chen*[1,3*], *Yue Lin*[4], *Lei Shi*[4], *He Lin*[5], *Xingyu Gao*[5], *Xingmin Zhang*[5], *Hang Chi*[6] and *Ctirad Uher*[6]

[1]Dr. Huili Liu, Xun Yuan, Ping Lu, Ying He, Prof. Xun Shi, Fangfang Xu, Wenqing Zhang, Lidong Chen
State Key Laboratory of High Performance Ceramics and Superfine Microstructure, Shanghai Institute of Ceramics, Chinese Academy of Sciences, 1295 Dingxi Road, Shanghai 200050, China.
E-mail: xshi@mail.sic.ac.cn; wqzhang@mail.sic.ac.cn; cld@mail.sic.ac.cn

[2]Dr. Huili Liu, Xun Yuan, Ping Lu, Ying He
University of Chinese Academy of Sciences, Beijing 100049, China.

[3]Prof. Xun Shi, Lidong Chen, Mr. Yunshan Tang, Dr. ShengqiangBai
CAS Key Laboratory of Energy Conversion Materials, Shanghai Institute of Ceramics, Chinese Academy of Sciences, 1295 Dingxi Road, Shanghai 200050, China.

[4]Dr. Yue Lin, Lei Shi
Hefei National Laboratory for Physical Sciences at the Microscale, University of Science and Technology of China, Hefei, Anhui 230026, China

[5]Prof. He Lin, Xingyu Gao, Dr. Xingmin Zhang
Shanghai Synchrotron Radiation Facility, Shanghai Institute of Applied Physics, Chinese Academy of Sciences, 239 Zhangheng Road, Shanghai 201204, China.

[6]Dr. Hang Chi, Prof. Ctirad Uher
Department of Physics, University of Michigan, Ann Arbor, Michigan 48109, USA.

This supporting information includes:

Computational Details:

All calculations were carried out using Vienna ab initio simulation package (VASP)[1]. The PAW method[2] and PBE[3] exchange-correlation functional were used. The low temperature phase was obtained by structural relaxation from high temperature cubic β-phase. Firstly, the phonon spectrum of cubic β-phase was calculated and some soft vibrational modes (i.e., with imaginary frequencies) were found at some special k-points. Different supercell structures of the β-phase were then constructed with initial atomic displacements according to the soft modes and then relaxed to obtain lower-energy structures. We identified out one monoclinic structure and one triclinic structure with nearly the same low energies, having very similar local structural characters. These structures have tiny structural differences and are proposed to compose the α-phase at room temperature. The structural parameters of the monoclinic and triclinic structures are listed in **Table S1** and **S2** respectively. They display almost the same behaviour during the phase transition. Thus only the monoclinic structure is shown in the main text. The transition path from the α-phase to the cubic β-phase (see Figure 3f) is calculated using a nudged elastic band (NEB) method[4] in which twelve transition images between the structures of α and β phases were considered. No energy barriers are observed during the transition from the monoclinic α-phase to the β-phase, indicating a typical behaviour of a second-order phase transition in Cu_2Se.

SEM and TEM Analysis:

Figure S3 shows the SEM image of Cu_2Se bulk sample sintered by SPS. **Figure S4** shows the diffraction patterns of Cu_2Se during a monoclinic-cubic phase transition. L2 and L3 core-loss edges of a transition metal in EELS carry information about oxidation states owing to the change in 3d states occupancy. The fine structure of copper in nonzero oxidation states (see **Figure S5**b and S5c), such as Cu^+ or Cu^{2+}, shows intense sharp L2 and L3 edges (white lines), whereas Cu^0 shows only broad edges. The energy of Cu L2 and L3 core-loss slightly differs with the chemical valence, i.e. $Cu^+<Cu^{2+}<Cu^0$. A mixture of Cu oxidation states obtained from the experimental EELS fine structure of the present Cu_2Se sample is shown (Figure S5a). Broad edges indicate the dominant state of metallic Cu, while a sharp peak and a small shoulder at its left side suggest the presence of Cu^{2+} and Cu^+ species, respectively. The EELS result matches well with the proposed structural model of the low temperature phase, where both Cu-Cu and Cu-Se bonds exist while the former dominates.

XRD and Thermoelectric Properties:

The XRD data for bulk samples sintered by SPS is shown in **Figure S6**. It is similar to the data of powders (ref. 15 in the main text), suggesting the random distribution of grains in bulk samples. This is further confirmed by SEM image shown in Figure S3**,** where the bulk samples in macroscale comprise of randomly distributed plate-shaped grains around a few hundreds nano-meters. Similar to layered TE material Bi_2Te_3 (ref. 13 in the main text), the nanostructures tend to form highly non-textured structures, thus to show isotropic transports. Calculations of the thermopower using Eq. 3 are consistent with the experiment data (see Figure 2a). The fitting parameters for calculations are listed in **Table S3**. Here, the T_0 and T_C values agree nicely with DSC measurements (see Table S3). The carrier concentration (p) and carrier mobility (μ_H) were calculated by the formula $p = 1/(R_H e)$ and $\mu_H = 1/(pe\rho)$, here e is electronic charge and R_H is the measured Hall coefficient. The electrical thermal conductivity (κ_e) is calculated by $\kappa_e = L_0 T/\rho$, where L_0 is the Lorentz number. Lattice thermal conductivity κ_L is calculated by $\kappa_L = \kappa - \kappa_e$. The Lorentz number could be significantly changed during phase transitions and the temperature dependent values are not known yet. Here, if a constant Lorentz number such as 1.3×10^{-8} V^2K^{-2} is used, κ_L is hugly decreased during phase transitions (**Figure S7)**, indicating very strong phonon scattering.

Thermoelectric Cooling Devices:

A device (thermoelectric couple), shown in **Figure S8**, was constructed and tested to measure its cooling ability. It consists of a p-type leg of Cu_2Se (left leg in Figure S8) with an n-type leg (right leg) made of Yb single-filled skutterudite. A thin Ni layer is plated on the top and bottom surfaces of thermoelectric materials using Electroplating method to ensure low resistance contact between the thermoelectric materials and metals. A thin Ni plate with two welded K-type thermocouples is soldered on the top junction of the couple to measure the temperature of the cold junction side (T_{CJ}). Two copper pieces (5.5mm in height) are soldered on the bottom surfaces of thermoelectric materials with another two welded K-type thermocouples to measure the temperature of the heat sink side (T_S). This single TE couple is soldered on a Al_2O_3 plate with well-designed copper electrodes on its surface, and then mounted on a massive copper cylinder with its bottom side inserted into the center of a small furnace. The temperature of this device is then controlled by this small furnace. Testing of this device is performed in a vacuumed chamber under the pressure of 10^{-4} torr at a few selected temperatures to cover α-phase, β-phase, and the phase transition region of Cu_2Se. When dc current (I) is passed through the TE couple, the temperature at the top junction (cold junction) is quickly reduced due to the Peltier effect. The maximum temperature drop (ΔT) with respect to the cold junction temperature T_{CJ} for selected currents is shown in **Figure S9**[5].

$$\Delta T = \frac{(S_p - S_n) I T_{CJ} - \frac{1}{2} I^2 R}{K} \quad \text{(S1)}$$

Where S_p and S_n are the thermopowers of Cu_2Se and Yb-filled skutterudite, respectively. R and K are the total electrical resistance and thermal conductivity of the device, respectively. When current (I) is small, the term $\frac{1}{2} I^2 R$ could be neglected. Thus the cooling ability of the device could be described by the parameter of $\Delta T/T_{CJ}$.

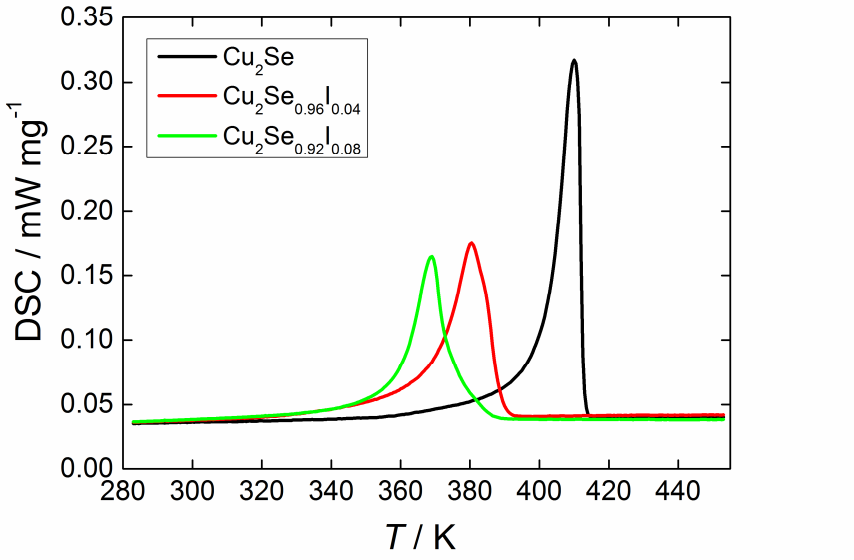

Figure S1. Differential Scanning Calorimetry (DSC) measurements for $Cu_2Se_{1-x}I_x$. The starting onset temperature (T_0) and the critical point (T_C) of the phase transition are estimated based on the measured DSC signals.

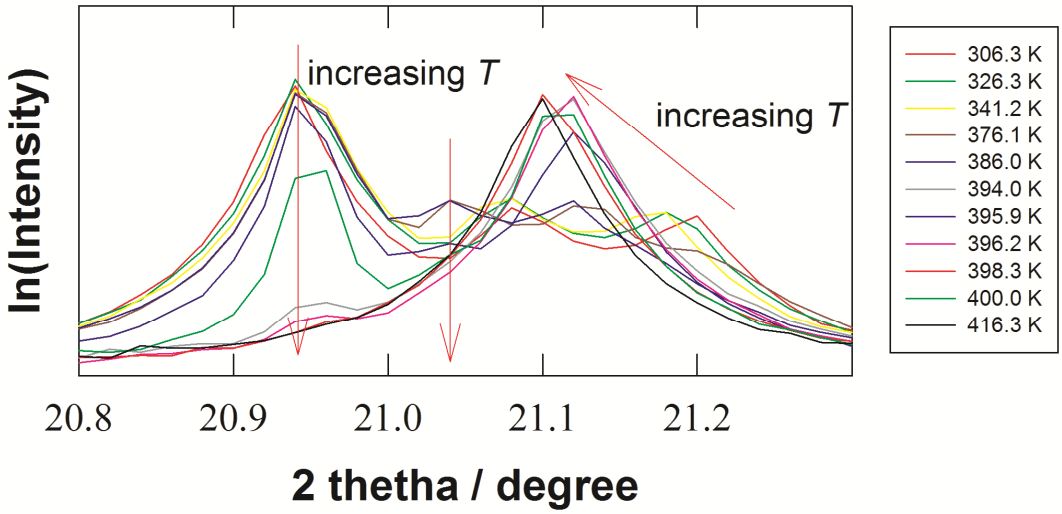

Figure S2. Intensity variation with temperature determined by SRLC measurements. The red arrows indicate the direction of heating the sample.

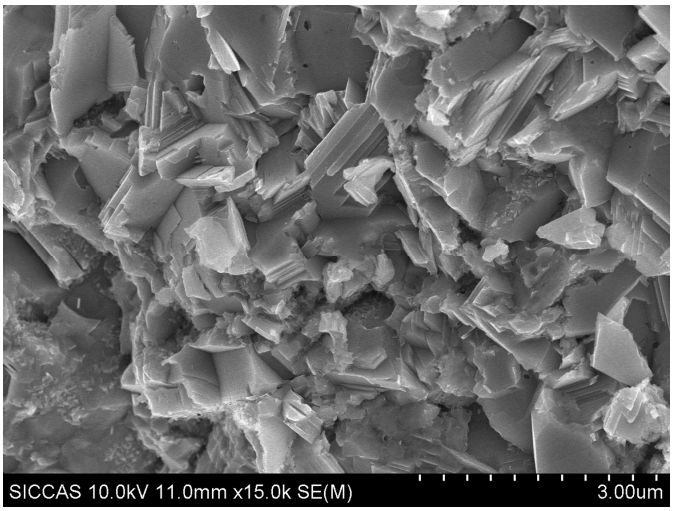

Figure S3. SEM image of Cu_2Se bulk sample sintered by SPS.

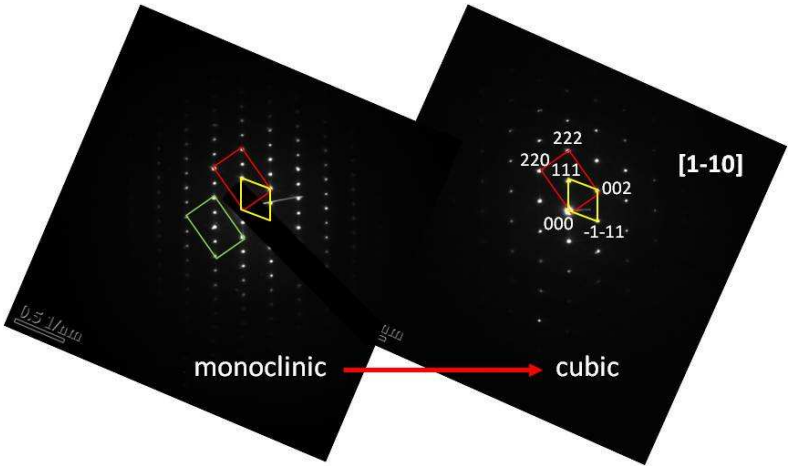

Figure S4. Diffraction patterns of Cu_2Se.

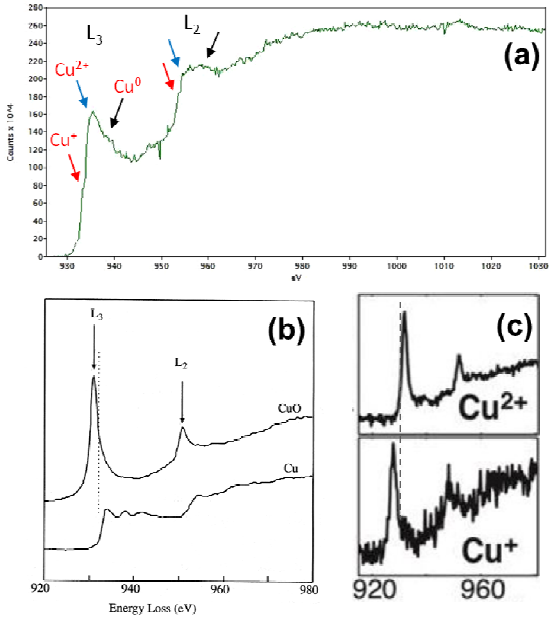

Figure S5. L2 and L3 core-loss edges of a transition metal in EELS for Cu_2Se. Figures S5b,c are taken from refs. 6 and 7.

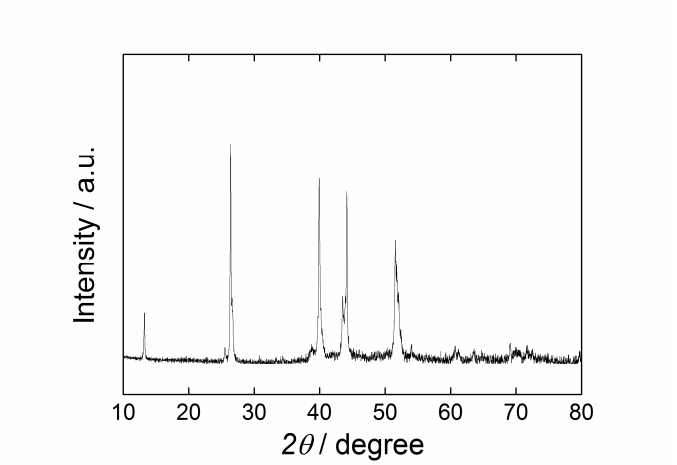

Figure S6. XRD data of Cu_2Se bulk sample sintered by SPS.

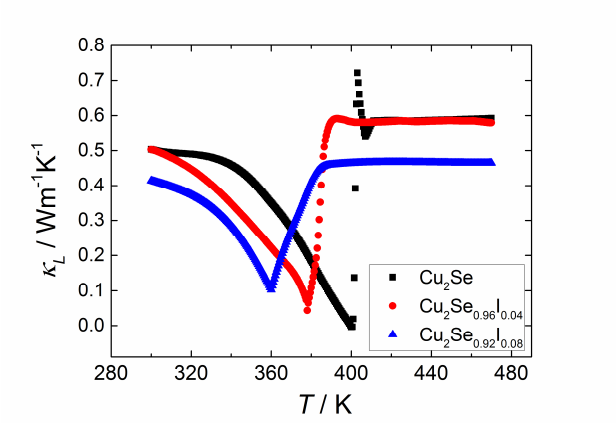

Figure S7. Temperature dependence of lattice thermal conductivities of bulk Cu_2Se sample sintered by SPS.

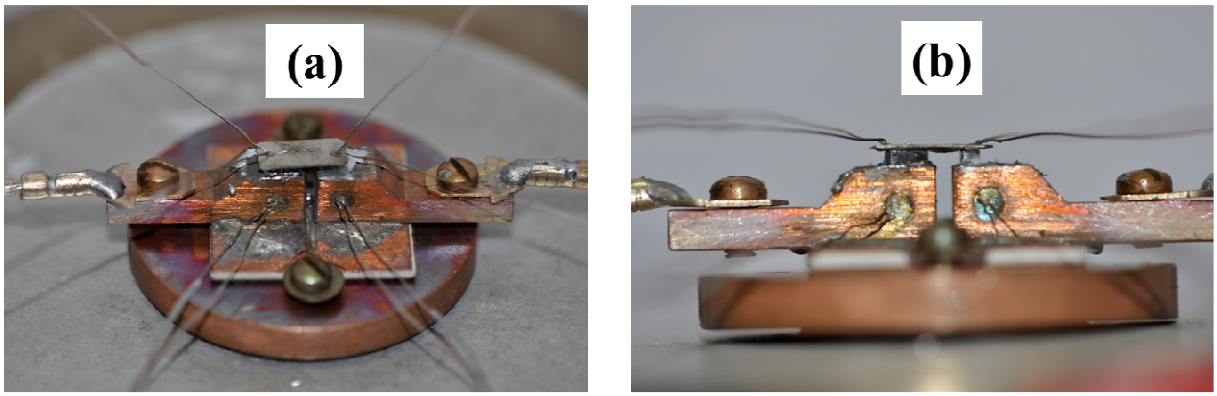

Figure S8. Experimental setup of the cooling device using Cu_2Se as a p-type leg (left leg) and n-type Yb-filled skutterudite as an n-type leg (right leg). a) An overall view of the cooling device mounted on a copper cylinder which is inserted into the furnace. b) An enlarged picture of the TE couple and its mounting on the copper heat sink.

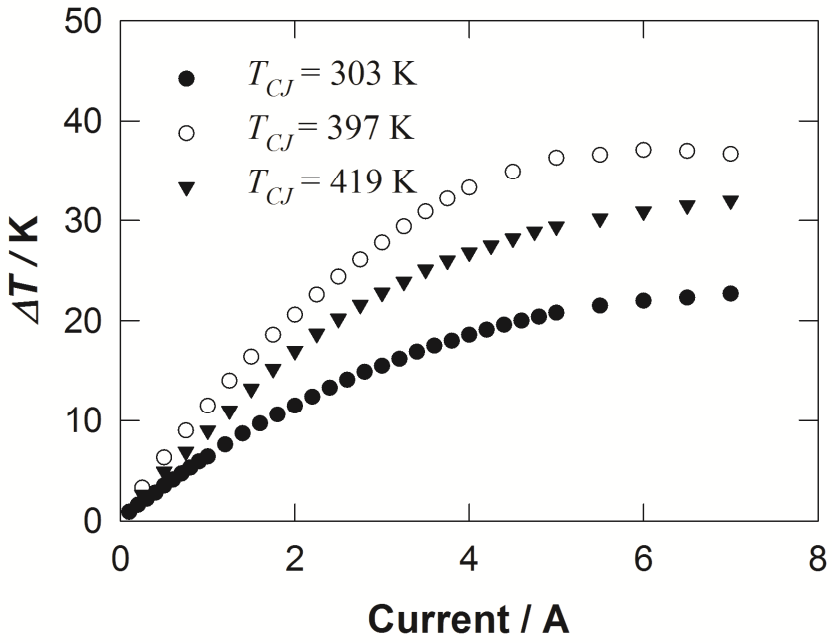

Figure S9. Cooling test results using the device shown in Figure S8 at different temperatures of the cold junction side, T_{CJ}.

Table S1. Structural parameters of low-energy monoclinic structure (space group: C2/c; #15) with *a*=7.130Å, *b*= 12.361Å, *c*= 14.466Å, and β=100.411°.

Atom	*x/a*	*y/b*	*z/c*
Cu1	0.78092	0.91802	0.58831
Cu2	0.28329	0.75077	0.59324
Cu3	0.30249	0.08388	0.64684

Cu4	0.01569	0.90117	0.47030
Cu5	0.57869	0.78660	0.46937
Cu6	0.62173	0.06211	0.46906
Se1	0.36111	0.91572	0.35798
Se2	0.36844	0.24731	0.36101
Se3	0.86835	0.08446	0.36025

Table S2. Structural parameters of low-energy triclinic structure (space group: P-1; #2) with *a*=7.120Å, *b*= 7.1371Å, *c*= 7.507Å, α=98.646°, β=107.689°, and γ=60.112°.

Atom	*x/a*	*y/b*	*z/c*
Cu1	0.72262	0.66477	0.67792
Cu2	0.06059	0.99675	0.68533
Cu3	0.42783	0.33115	0.79105
Cu4	0.35536	0.69827	0.44182
Cu5	0.67997	0.92505	0.44216
Cu6	0.90632	0.37872	0.43826
Se1	0.91521	0.66897	0.22399
Se2	0.24070	0.00507	0.22213
Se3	0.57558	0.33086	0.21578

Table S3. Fitting parameters using Eq. 3 for $Cu_2Se_{1-x}I_x$ samples. The T_0 and T_C values are estimated by fitting the measured thermoelectric (TE) properties. The data estimated by DSC signals are listed for data comparison.

	S_0(μVK^{-1})	ρ_C (ohm m)	A(μVK^{-2})	δ	T_0 (K)		T_C (K)	
					TE	DSC	TE	DSC
Cu_2Se	104.4	2.50×10^{-5}	0.1531	1.05	360	360	400	400
$Cu_2Se_{0.96}I_{0.04}$	100.8	3.84×10^{-5}	0.098	1.05	342	341	378	372
$Cu_2Se_{0.92}I_{0.08}$	168.0	11.13×10^{-5}	0.0681	1	342	341	360	360

[1] G.Kresse, J. Furthmüller, *Phys. Rev. B* **1996**, *54*, 11169.
[2] G.Kresse, D. Joubert, *Phys. Rev. B* **1999**, *59*, 1758.
[3] J. P.Perdew, K.Burke, M. Ernzerhof, *Phys. Rev. Lett.* **1996**, *77*, 3865.
[4] G.Mills, H.Jonsson, G. K. Schenter, *Surface Science*, **1995**, *324*, 305.
[5] G. S. Nolas, J. Sharp, H. J. Goldsmid, in Thermoelectrics: basic principles and new materials developments, (Eds: A. Zunger, R. M. Osgood Jr, R. Hull, H. Sakaki), Springer Verlag, New York 2001, Ch. 1.
[6] C. C.Ahn, O. L. Krivanek, *EELS Atlas*. ASU HREM Facility and GatanInc, 1983.
[7] K. J.Koski, J. J.Cha, B. W.Reed, C. D.Wessells, D. S.Kong, Y.Cui, *J. Am. Chem. Soc.* **2012**, *134*, 7584.